Article

Effective Regulation of ZnO Surface Facets for Enhanced Photoluminescence Properties Assisted by Zinc Quaternary Ammonium Salts

Bo Song,[⊥] Yun Xie,[⊥] Xia Cui, Guangyao Zhan, Jing Mao, Changzeng Fan, Yijiang Shao,* Yueming Sun, and Yuqiao Wang*

ACCESS | 📊 Metrics & More | 📖 Article Recommendations | 🆂🅸 Supporting Information

ABSTRACT: Novel ZnO twined-mushroom structures highly exposed in $(00\bar{1})$ planes were fabricated via a facile solvothermal synthesis with assistance of a zinc quaternary ammonium salt in the methanol−water solvent to show enhanced photoluminescence properties. A series of ZnO morphologies regulated with different surface facets were obtained in both MeOH−H$_2$O and EtOH MeOH−H$_2$O solvents respectively, tuning the proportion of alcohol. The self-aggregation mechanism was proposed based on the time-controlled experiment to evaluate the formation of twined-mushroom structures. The selective adsorptions of anions from zinc salt precursors determine the shape of subunits and direct the subunits, which act as building blocks to form the order aggregations.

Morphology Regulation

INTRODUCTION

In past decades, ZnO has attracted immense attention of the researchers due to its unique physical, chemical, and optical properties ascribed to its variable morphologies from zero-dimensional (0D) to three-dimensional (3D) structures.[1−4] Consequently, ZnO is widely applied in many fields, such as chemical sensors,[5] lithium ion batteries,[6] solar cells,[7] and optical devices.[8−10] All of these promising usages attract great interest among people to develop various synthetic strategies, including solution methods,[11] chemical vapor deposition,[12] aqueous pathway,[13] and so on. The solution methods are simple, powerful, and convenient due to easy tuning of the experimental conditions to control the crystal growth process and selectively synthesize various morphologies for better use. Especially, the solvothermal method is currently an effective strategy because it allows the formation of a variety of ZnO morphologies assisted by different organic reagents.[14]

The ZnO crystal is often considered as a sequence of hexagonal ZnO units composed of alternating staking of 4-fold tetrahedrally coordinated Zn^{2+} and O^{2-} ions connected alternatively along the *c*-axis.[15−17] Thus, the ZnO hexagonal prism is made up of the Zn^{2+}-terminated (001) and O^{2-}-terminated $(00\bar{1})$ polar faces as well as six nonpolar Zn^{2+} and O^{2-} co-terminated prismatic faces. The growth rates of each face determine the final morphology of ZnO crystals. However, crystallization is usually interfered by the species dissolved in the reaction solution as the nucleation and growth processes are sensitive. Therefore, additives are introduced into the ZnO crystal growth to either impede or promote further growth of the different faces. The additive-assisted synthesis of mediating ZnO growth is a very promising strategy to vary the ZnO

structure, resulting in a wide variety of curious morphologies of ZnO.[18,19]

ZnO crystals highly exposed in $\pm(001)$ facets are desired for enhancing their performance in many applications in view of various properties of ZnO with different crystal faces.[20−23] Mostly, single ZnO crystals exposed in $\pm(001)$ faces could be synthesized by using additives to inhibit the growth rate along the [001] direction for forming a two-dimensional (2D) structure. The ZnO mesocrystals are stacked with lamellar structures exposed in $\pm(001)$ planes as building blocks.[24,25] More complex ZnO twin spheres exposed in $\pm(001)$ facets were prepared by introducing organic additives.[8] Herein, ZnO twined mushrooms exposed in $(00\bar{1})$ planes were fabricated via a facile solvothermal synthesis in the methanol−water solvent using zinc *N*-dodecyl-*N*,*N*-dimethylammonioacetic bromide $(Zn(DDAB)_2)$[26] as a zinc salt precursor.

EXPERIMENTAL SECTION

Synthesis of ZnO Twined Mushrooms in Methanol (MeOH)−H$_2$O System. A high concentration of 0.25 M Zn(DDAB)$_2$ solution was prepared with reference to our previous work.[26] Then, this solution was diluted to 0.0125 M with mixed solvents of MeOH and deionized water. The volume fractions of MeOH in the reaction mixtures were

controlled to vary from 80 to 95%. Hexamethylenetetramine (HMTA) with an equal molar ratio of Zn^{2+} was dissolved in the above mixtures under stirring to form transparent solutions. Subsequently, these solutions were transferred to Teflon-lined steel autoclaves where clear fluorine-doped tin oxide (FTO) glass substrates were put beforehand for deposition and heated at 105 °C for 12 h. Besides the substrates, the white precipitates deposited at the bottom were also collected by centrifugal separation, washed with MeOH several times, and then kept at 60 °C in vacuum for 12 h.

Synthesis of ZnO Twined Spheres in Ethanol (EtOH)−H₂O System. The 0.25 M $Zn(DDAB)_2$ solution was diluted to 0.0125 M with mixed solvents of EtOH and deionized water. The volume fractions of EtOH in the reaction mixtures varied from 80 to 95%. The subsequent procedure for preparation of ZnO was the same as in the MeOH−H₂O system.

Characterization Studies. The purities and crystal structures of the collected products were detected by powder X-ray diffraction (XRD) on a Rigaku Smartlab 3 with monochromatized Cu Kα radiation. Scanning electron microscopy (SEM, FEI), transmission electron microscopy (TEM, JEM-2100), and high-resolution transmission electron microscopy (HRTEM) were used to investigate the morphologies and microscopic features of the samples. Room-temperature photoluminescence (PL) spectra of different shapes of ZnO were conducted on a HORIBA FluoroMax-4 fluorescence spectrophotometer at an excitation wavelength of 345 nm. Electrochemical impedance spectroscopy (EIS) was performed on the electrochemical workstation (CHI 660E) at a bias voltage of 5 mV in a frequency range from 10^{-1} to 10^5 Hz.

■ RESULTS AND DISCUSSION

The XRD patterns in Figure 1 indicate that all samples obtained from different concentrations of MeOH solvents are
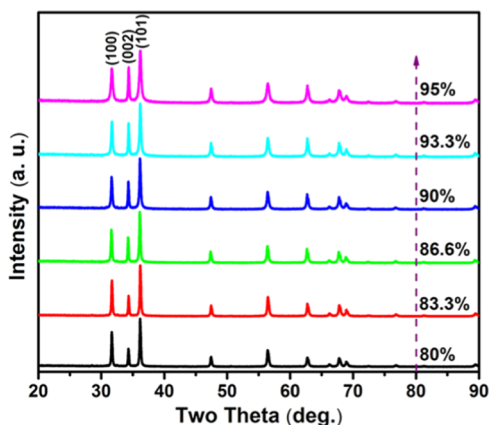
Figure 1. XRD patterns of the products obtained in the MeOH−H₂O solvents with varied volume fractions of MeOH.

well-crystallized hexagonal ZnO (JCPDS cards, No. 36-1451) without observation of characteristic peaks derived from any impurities, demonstrating the high phase purity of all samples. The relative intensities of the reflection peaks corresponding to the (002)/(100) facets increase significantly with increasing MeOH concentration (Table S1), indicating an incremental exposure of polar ±(001) faces of ZnO.[27] The crystallite sizes in the c- and a-axis (Table S1), namely, D_c and D_a, are deduced

from the full width at half-maximum (FWHM) of (002) and (100) peaks by the Scherrer formula. With increasing MeOH concentration, D_c changes slightly accompanied by a gradual decrease of D_a from 45.3 to 24.7 nm, leading to a significant increase of dimension ratios for the c- and a-axis. This phenomenon is similar to the observation of ZnO synthesized in ethylene glycol/water.[20] Therefore, it could be deduced that the increasing MeOH concentration interrupts the growth of each individual ZnO crystallite especially in the a-axis direction.

The SEM and TEM observations in Figure 2 further display the evolution of the typical morphologies and microstructures of ZnO generated from varied MeOH concentrations. In the 80 vol % MeOH solvent, the product is ZnO twined rods with slightly thinner waists and rounded tips (Figure 2 a1,a2). Distinguished from smooth prisms, the rods exhibit rough surfaces on which palpable grooves and tiny bulges are scattered. As the MeOH concentration increased to 83.3 vol %, the bulges on the surfaces grow into wedges of different sizes, which are aligned approximately parallel and wrapped successively in generations along the ends of each rod core (Figure 2b1,b2), forming a twined-bundle-like structure. With the increase of MeOH concentration, the ZnO surfaces are composed of incremental generations of the nonuniform wedges, forming the twined-pinecone-like structures (Figure 2c1,c2). On further increasing the MeOH concentration (Figure 2d1,d2), the drops of each generation became relatively uniform from the side view; in other words, the surfaces are covered with basically uniform wedges, resulting in pronounced arc outlines for the formation of twined-custard-apple structures. In the 93.3 vol % MeOH solvent (Figure 2e1,e2), ZnO appears similar to twined-custard-apple-like structures but with smaller sizes. The difference is thinning down of the wedges and changing into small facets, which link with each other via tilting step-by-step to form the scaly and curved surfaces of the twined-custard-apple structures. The sizes of the small facets are further reduced and packed much tightly to form twined-mushroom-like structures after further increasing the MeOH concentration to 95 vol % (Figure 2f1,f2). It is worth noting that the morphologies generated in different solvents in Figure 2 are representative and dominant in large scale (Figure S1), although tiny amounts of unexpectedly impure shapes are observed. All products consist of two halves joined together at their concave waists. TEM images (Figure 2a3−f3) clearly display the general trends of morphological evolutions with the increase of MeOH concentration from 80 to 95 vol %. A general downward trend is exhibited on the individual sizes including the maximum width, waist width, and longitudinal length. Meanwhile, the curve profiles of the individual surfaces increase gradually, leading to a variety of morphologies.

ZnO obtained in the 95 vol % MeOH solvent shows a uniform twined-mushroom-like structure with maximum exposure of polar ±(001) faces. Figure 3A exhibits the TEM image of a typical twined-mushroom particle, consisting of two mushrooms, which are composed of half-sphere and truncated cone united symmetrically at a common base as marked with a red arrow. for an indepth understanding of the microscopic surface structure, HRTEM observations (Figure 3a−g) are taken clockwise around the spherical surface of the twined mushroom at different locations, marked with blue rectangles in Figure 3A. The lattice fringe spacings in these HRTEM images are about 0.26 nm, calculated from the fast Fourier
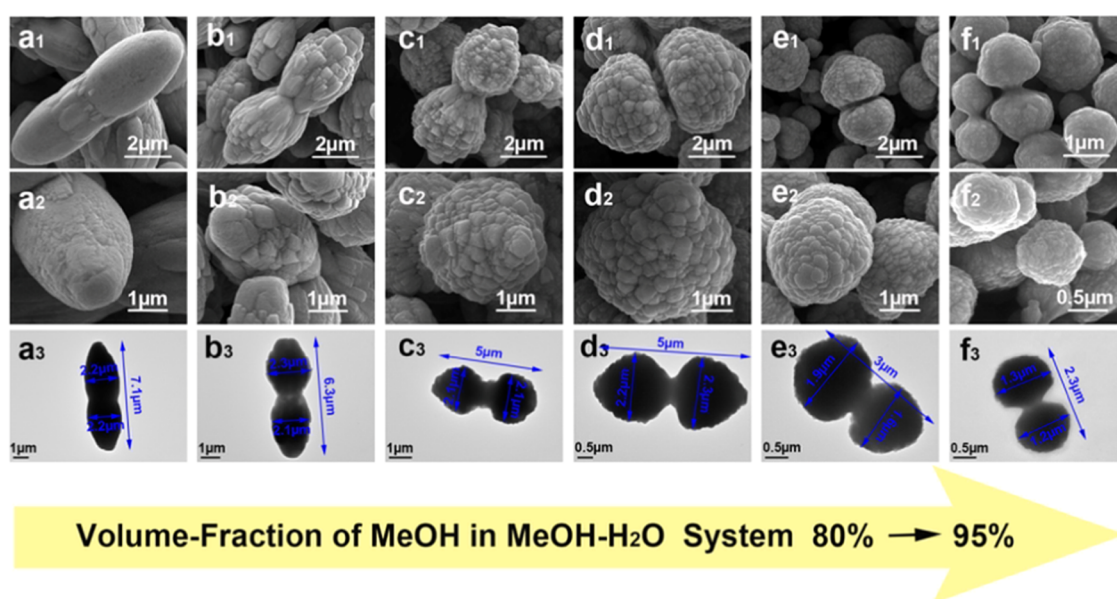
Figure 2. SEM images of side and top views and TEM images of ZnO prepared in different vol % of MeOH in MeOH−H$_2$O solvents. (a1−a3) 80 vol % MeOH, (b1−b3) 83.3 vol % MeOH, (c1−c3) 86.6 vol % MeOH, (d1−d3) 90 vol % MeOH, (e1−e3) 93.3 vol % MeOH, and (f1−f3) 95 vol % MeOH.
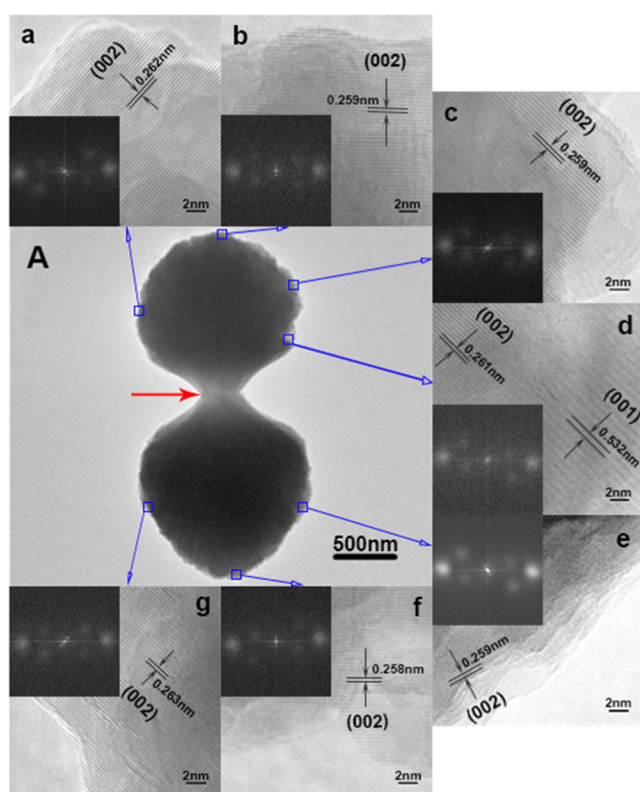
Figure 3. TEM and HRTEM images of ZnO synthesized in 95 vol % MeOH solvent. (A) TEM image of a typical ZnO twined mushroom, and (a−g) HRTEM images of the marked parts in (A) with indicated *d*-spacings calculated from the fast Fourier transform (FFT) analyses.

transform (FFT) analyses, corresponding to the interspacing of the (002) crystal facets of ZnO. Additionally, the lattice spacing of 0.532 nm indicated in Figure 3d is consistent with the *d*-spacing of (001) planes. In view of this, the spherical surfaces of ZnO twined mushroom are enclosed in polar ±(001) faces; that is, the ZnO twined mushroom should

display either negatively or positively charged surfaces because of the polar oxygen (00$\bar{1}$) or polar zinc (001) basal planes. This case had been substantiated via electrostatic staining in previous reports.[28,29] In our staining experiments, a negatively charged dye (Acid Green 25) and a positively charged dye (methylene blue) were introduced and their adsorption behaviors were investigated by visual inspection and SEM observation (Figure S2). Only the positively charged dye adsorbs on the spherical surfaces of the ZnO twined-mushroom structures, suggesting the feature of electro-negativity on their surfaces caused by the oxygen-terminated (00$\bar{1}$) planes. That is, ZnO twined-mushroom structures are exposed in (00$\bar{1}$) planes, and the percentage of exposed polar facets is estimated to be about 90%. Unexpectedly, the use of the negatively charged dye causes the structural damage of the twined mushrooms, which break down at the waist into mushroom structures, indicating that the twined-mushroom structures are composed of two mushrooms growing at a base plane in between. This twining phenomenon commonly occurs during the ZnO growth with the (001) or (00$\bar{1}$) plane as the juncture.[29,30] In line with the results reported previously, it could be deduced that the twined-mushroom structures grow along the [00$\bar{1}$] direction in both parts from the juncture, which is presumably formed via an initial alignment of (001) to (001) facets (probably mediated by the anion of Zn(DDAB)$_2$, namely, DDAB$^-$).

To further clearly observe the surface morphology of the ZnO twined mushroom, the high-magnification SEM image is recorded as shown in Figure 4a, which displays the top view of one twined mushroom and the side view of a defective ZnO twined mushroom. The top view reveals that the spherical surfaces are covered by the tiny facets with recognizable edges and corners. As highlighted in red lines, the measured angles of the two corners of an individual facet are 119 and 119.3°, respectively. The above XRD pattern (lilac pattern in Figure 1) and HRTEM images (Figure 3) indicate that the twined mushrooms are indexed to hexagonal ZnO and exposed in polar (00$\bar{1}$) planes; hence, it could be concluded that the facets
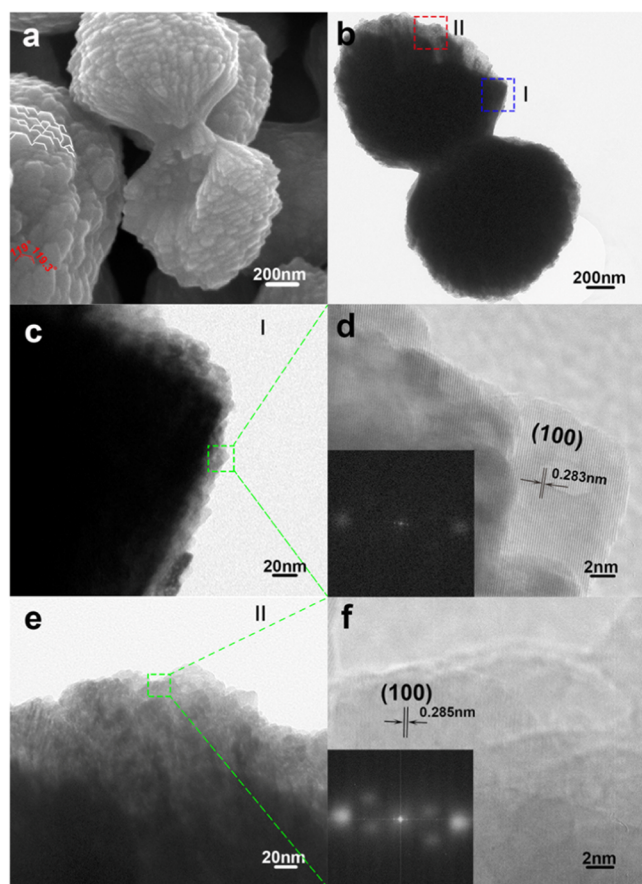
Figure 4. (a) SEM image of top and side view of ZnO twined mushroom, (b) TEM image of a defective ZnO twined mushroom, (c, e) magnified TEM images of the parts in (b), and (d, f) HRTEM images with indicated *d*-spacings calculated from the FFT analyses of the parts in (c) and (e).

are partial hexagons with O^{2-}-terminated planes. The side view of a defective twined mushroom reveals the growth habit of the ZnO structure. It is clearly seen that the twined-mushroom structure is composed of ZnO nanowedges of 20−100 nm size. The wedge-shaped morphology tapering toward the inside is relatively visible in a fragment (Figure S3a). These nanowedges attach to each other tightly and radiate outward on both sides from the basal plane in between. Obviously, this formation of the twined-mushroom structure proceeds via an oriented aggregation of initially formed subunits proposed by Cölfen,[31] rather than the classical ion attachment. We assume that the DDAB− anions are incorporated in the formation of the twined-mushroom structure. This conjecture is evidenced by the thermogravimetric analysis, which indicates that the twined-mushroom-like ZnO contains approximately 4% of organic material (Figure S3b).

Further TEM observation is to investigate the arrangement of the subunits. Figure 4b shows a typically defective ZnO twined mushroom with a visible breach in itself. Two parts, respectively, marked with blue (I) and red (II) dashed lines on the breach are magnified as displayed in Figure 4c,e, indicating fairly rough brim, presumably caused by the aggregation of ZnO wedges on the breach and the conical surface. Figure 4d shows the HRTEM image of the side part on the conical surface as marked in Figure 4c. Figure 4f exhibits the HRTEM image of the top part on the breach as marked in Figure 4e.

The lattice fringe spacing of about 0.28 nm calculated from the FFT analyses (Figure 4d,f) corresponds to the interspacing of (100) plane of ZnO. The sizes of the nanowedges are estimated in a range of 20−30 nm, which is in agreement with the calculated result from the XRD analysis (Table S1). In addition, the degrees of the orientational alignment of the nanowedges consist of the (100) planes located at the same part. Hence, it could be deduced that the orientational aggregates of the nanowedges radiate outward with regard to their *c*-axis.

To further clarify the formation of the ZnO twinned-mushroom structure, a time-dependent experiment was conducted in the 95 vol % MeOH solvent and the products were collected after defined time intervals for further XRD and SEM investigations (Figure 5). The XRD patterns (Figure 5a)
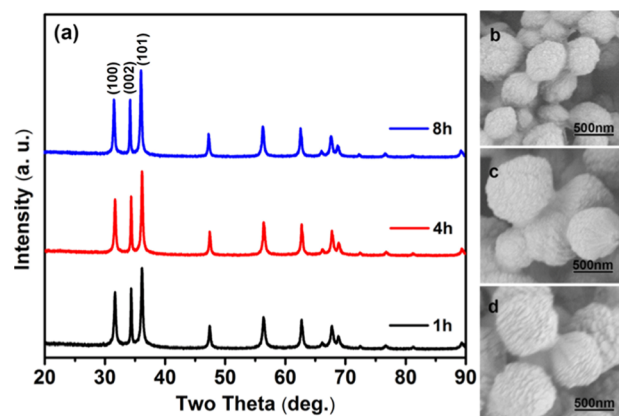
Figure 5. (a) XRD patterns and (b−d) SEM images of the products obtained at different reaction times in 95 vol % MeOH solvent. (b) 1 h, (c) 4 h, and (d) 8 h.

display the fast crystallization of ZnO. Even if the sample was collected after a short reaction time of 1 h, pure ZnO with high crystallinity is observed. Prolonging the reaction time, there is scarcely any change in the purity and crystallinity of ZnO. Focusing on the individual crystallites, their crystallite sizes D_c and D_a are estimated from the FWHM of (002) and (100) diffraction peaks using the Scherrer formula. As provided in Table S2, the subunits of the sample collected at 1 h show the thinnest rod/wedge-like habit with D_c of 42.2 nm and D_a of 20.5 nm. A slow growth of the subunits in both directions proceeds with the increase in the reaction time, and the growth in *a*-axis dominates relatively, leading to a gradual decrease of dimension ratio for the *c*- and *a*-axis. That is, the subunits become thicker with time and their growth appears to be completed after 8 h of reaction.

The morphology evolution of these samples is monitored with SEM images (Figure 5b−d). The formation of the twined-mushroom-like structure proceeds within a short period of time. This typical morphology appears at the early stage of the reaction with relatively small dimensions of ∼0.54 *μ*m width and 1.07 *μ*m longitudinal length (Figures 5b and S4a). With increasing reaction time, the sizes of the subunits are increased as mentioned above, resulting in further growth of the twined-mushroom structure whose size is up to about 0.87 *μ*m in width and 1.6 *μ*m in longitudinal length (Figures 5d and S4c). With the increase in the size of the twined-mushroom structure, however, the amount of the aggregated subunits is relatively constant in appearance. Consequently, the

Scheme 1. Schematic Illustration of the Formation of the ZnO Twined-Mushroom Structure in 95 vol % MeOH Solvent
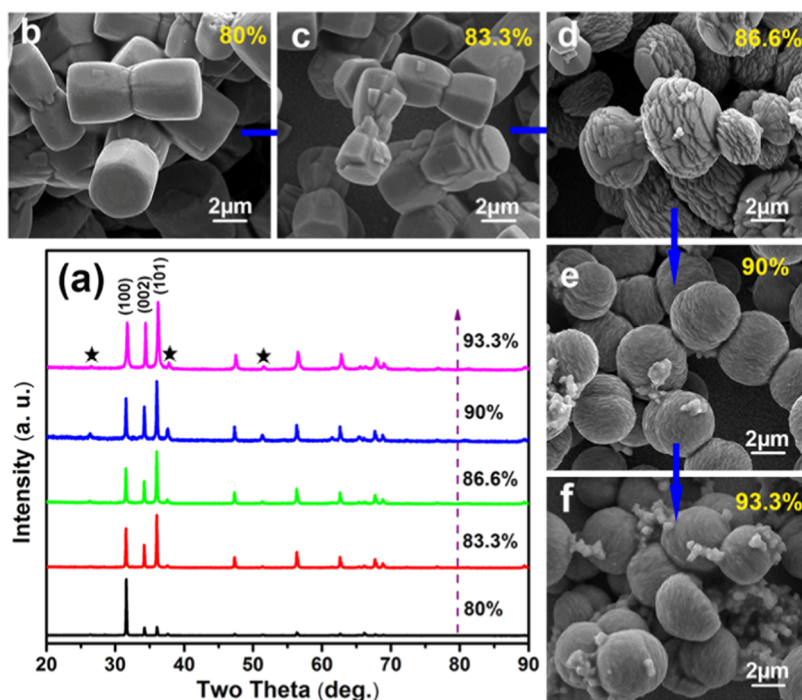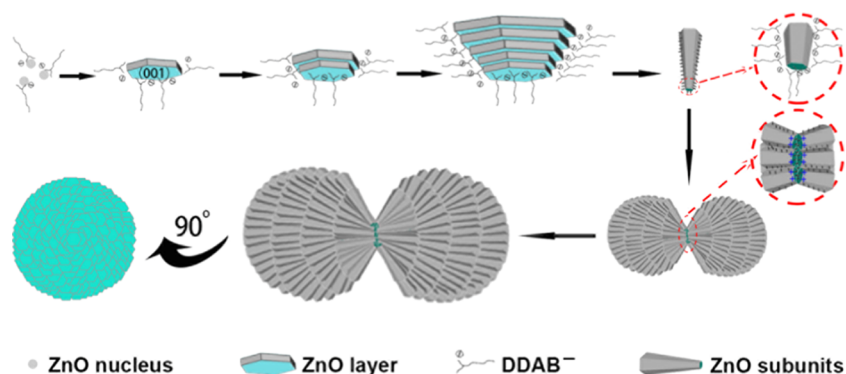
Figure 6. SEM images (a–e) and XRD patterns (f) of the samples synthesized in different vol % of EtOH in EtOH–H$_2$O solvents: (a) 80 vol % EtOH, (b) 83.3 vol % EtOH, (c) 86.6 vol % EtOH, (d) 90 vol % EtOH, and (e) 93.3 vol % EtOH.

growth of the structure presumably proceeds with the growth of individual subunits rather than further adjoining of crystallites.

In consideration of the observation and analysis mentioned above, a formation mechanism is postulated for the ZnO twined mushroom as depicted in Scheme 1. Commonly, HMTA could be hydrolyzed in water to provide a continuous release of OH$^-$ with increasing temperature.[32−34] Although the solvent used in the experiment was mainly composed of methanol, there was still a little water in the solvent for reaction with HMTA of which self-hydrolysis might be restrained and slowed to an extent. In addition, the EIS measurement indicates that the ionization equilibrium existed between the Zn(DDAB)$_2$ precursors in the MeOH–H$_2$O solvent, forming Zn^{2+} and DDAB$^-$ ions with coexistence of partial zinc salt molecules (Figure S5).

With OH$^-$ ions being slowly generated from HMTA at an initial stage, ZnO nuclei are formed and modified by DDAB ions, preventing themselves from aggregation. Analogously, ZnO nanocrystals have been reported previously to be stabilized by the anions composed of ionic liquid salts containing Zn^{2+} cations.[35,36] And then, the defined crystal faces are developed to incubate the hexagonal ZnO units as the basic growth layers when OH$^-$ ions are gradually released from HMTA. As Zn^{2+} ions are consumed for forming ZnO, the ionization of zinc salt could be promoted to release dissociative DDAB$^-$ ions, which act as in situ capping agents to coordinate in steps to the tetrahedral Zn^{2+} ions exposed on the unit surfaces.[26] As a result, DDAB$^-$ ions anchor onto Zn^{2+}-terminated (001) faces as well as Zn^{2+} and O^{2-} co-terminated prismatic faces, most likely with their polar head-groups bound to the surfaces and alkyl chain toward the outside,[37,38] causing the crystal growth inhibition along the [001] and [100] directions. That is, the preferential growth of O^{2-}-terminated (00$\bar{1}$) faces could be realized to have the highest growth rate.

The crystal growth along the [00$\bar{1}$] direction could be considered as an orientational stacking of hexagonal ZnO units layer by layer along the c-axis, like the graphite structure.[16] When new ZnO hexagonal layers are generated on the basic growth layers, it is time for DDAB$^-$ ions to bind to the

nonpolar prismatic faces of the new layers, thus forming larger dimension of the new layers than that of basic layers. As each new layer generated with bigger dimension, the wedge-shaped ZnO subunits as building blocks for further aggregation would be formed predictably after tens of generation of the new layers. Meanwhile, the twinning structure occurs at an early stage by attaching the wedge-shaped ZnO subunits to themselves via the (001) faces. DDAB$^-$ ions binding to the (001) faces could possibly overcompensate and counterbalance the like charges on their facets,[28] allowing the appearance of twinning. Besides, the subunits are arranged side by side with each nonpolar surface, resulting in the formation of radiating aggregates due to the wedge shape of individual subunit (Figure S3a). Further aggregation of ZnO wedges would be carried through the stacking of the (001) faces on (00$\bar{1}$) faces exposed on the radiating aggregates, forming the twined-mushroom-like structures (Figure 5b). The aggregating process seems to be completed at an early stage; that is, the number of subunits in the aggregates nearly remain constant for a long period (Figure 5b,c). Hence, further growth of the aggregates is considered to be the individual growth of each subunit. With slow coarsening of the subunits (Table S2), the radian of the profile of aggregates becomes more round, forming the typical twined mushrooms exposed in the (00$\bar{1}$) facets in maximum (Figure 3).

It is well known that the property of the dissolvent would change the nucleation and growth rates of crystallites to determine the final morphologies. In the series of MeOH–H$_2$O solvents, the increasing proportion of water could accelerate the self-hydrolysis of HMTA, promoting the nucleation and incubation of the hexagonal ZnO basic growth layers at an initial stage. Meanwhile, less inhibition of ionization of the Zn(DDAB)$_2$ precursor allows local supersaturation of Zn^{2+} ions for ZnO nucleation and more DDAB$^-$ anions to bind fast to the nonpolar prismatic faces of the newly ZnO generated layers, leading to the new layers being similar in diameter to the basal layers. As a result, the subunits formed after tens of generation of the new layers change their shape gradually from wedge shape to rod shape, accompanied by the increase of the crystallite sizes in a-axis (Table S1) with increasing proportion of water in the MeOH–H$_2$O solvents. Predictably, the morphological evolution of the final structures aggregated by these subunits as building blocks proceeds from twined mushrooms to the twined-rod structure, which is less exposed in polar faces (Figures 1 and 2).

To confirm the validity and universality of the mechanism presented above, parallel experiments were conducted by replacing MeOH with EtOH and keeping the other reaction conditions unchanged (Figure 6). The XRD patterns shown in Figure 6a indicate good crystallinity and purity of all of the artefacts despite the impure diffraction peaks (marked with ★) arising from the FTO glass (Figure S6). With increase in the EtOH concentration, there is an obviously increasing tendency of the relative intensities of the diffraction peaks corresponding to the (002)/(100) planes (Table S3), indicating an increased exposure of polar facets. In addition, significant decreases of D_a and D_c are apparent with the increase of EtOH concentration; that is, the growth of each individual ZnO crystallite in both a- and c-axis direction is inhibited by the increasing concentrations of EtOH. At low EtOH concentration of 80 vol %, the twined-column structure of ZnO is observed with distinct and smooth prism surfaces (Figures 6b and S7a). Several wedges appear symmetrically on the prism facets around the twined

columns when EtOH concentration is increased to 83.3 vol % (Figures 6c and S7b). With further increase in the MeOH concentration (Figures 6d and S7c), a stem is observed after tens of generation of wedges growing around the side facets of the twined columns to connect two rough hemispheres for forming the dumbbell structure. The surface of the hemisphere is composed of a hexagonal plane at the top of the column and fragmentarily hexagonal facets at the top of the wedges. At the 90 vol % EtOH solvent (Figures 6e and S7d), twined-hemisphere structures are obtained with two hemispheres fused at the contracted central plane. The surface of the hemisphere is constructed by connecting each fragment through tilting step-by-step. When EtOH concentration is as high as 93.3 vol % (Figures 6f and S7e), the twined-hemisphere structure is maintained with much smaller fragments packed tightly to form relatively rounded surfaces. Some separated hemispheres are observed. Unexpectedly, the twined structures would be totally destroyed to form mushroom structures at higher EtOH concentrations (Figure S7f). Based on these observations, the evolution of crystal structures and morphologies of ZnO by regulating the content of alcohol in EtOH–H$_2$O solvents is almost the same as that in MeOH–H$_2$O solvents. Consequently, the orientational self-aggregation mechanism of forming twined-mushroom structures in MeOH–H$_2$O system is also suitable for the growth of the twined-hemisphere structures in EtOH–H$_2$O system.

PL spectra of the selected ZnO samples with varied morphologies are shown in Figure 7 to explore the influence
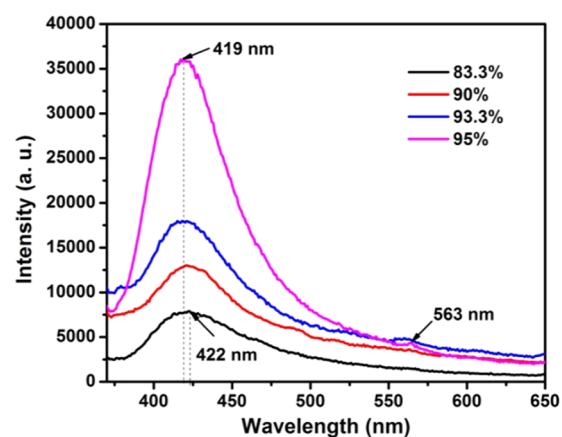
Figure 7. PL spectra of ZnO samples obtained in the MeOH–H$_2$O solvents with different MeOH concentrations.

of ZnO morphological regulation on its optical property. All samples exhibit obvious blue emission peaks at a wavelength of around 420 nm. The blue emission was also observed in other shapes of ZnO, such as hollow nanoparticles,[39] nanoshells,[40] flower-like rods,[41] and dumbbell-shaped microstructures,[42] suggesting that the PL property is influenced by the shape of ZnO.[43] Although the mechanism of excitation emission is controversial, the generation of the blue emission is commonly ascribed to the electron transition from the zinc interstitials (Zn$_i$) to the valence band and oxygen defects.[44−46] It is worth pointing out that the ZnO twined-mushroom structure exhibits almost 5-fold enhancement of PL intensities than the blue emission of the ZnO twined-bundle-like structure. That is, the morphological evolution for regulating exposed polar facets greatly influences the emission from the ZnO material. Two plausible reasons could be suggested to explain this emission

enhancement. One is the obvious increase of the percentage of exposed $(00\bar{1})$ facets via morphological evolution. The previous work on principal studies of ZnO indicated that the blue light could be emitted by $\pm(001)$ facets of ZnO, but the O^{2-}-terminated $(00\bar{1})$ facets emit much stronger blue light than the Zn^{2+}-terminated (001) facets.[47] Another one is that the ZnO subunits, which aggregated radially for the formation of the superstructures, are modified by the organic ions on their surfaces to lead to much more structural defects. In addition, a common green emission of ZnO at around 560 nm is negligible. Consequently, the strong blue emission confirms the twined-mushroom ZnO being a promising candidate in light-emitting devices, which require a monochromatic emission.

CONCLUSIONS

In summary, a series of well-controlled ZnO superstructures have been prepared via the MeOH−H_2O solvothermal method. ZnO morphologies evolving from twined rods to twined mushrooms were realized only by regulating the MeOH concentration from 80 to 95 vol %. Careful time-controlled experiments indicate that the $Zn(DDAB)_2$ precursor plays a crucial role in the formation of the twined-mushroom morphology. The cations of the precursor supply a constant zinc source for the ZnO crystal growth. The anions of the precursor, $DDAB^-$, act as capping agents to selectively adsorb on the primary ZnO crystallites to build subunits and synchronously aggregate orderly. Owing to the different ionizations of the $Zn(DDAB)_2$ precursor in these solvents, the concentration of $DDAB^-$ anions and their adsorption rates on primary crystals are influenced, resulting in different shapes of the subunits. Further growth is attributed to the slow growth of individual subunits. The morphological evolution, in particular, the increase of the exposed $(00\bar{1})$ facets, greatly enhances the PL property of ZnO. A similar morphological evolution from twined columns to twined hemispheres was also observed in EtOH−H_2O solvents by varying the EtOH concentration. This work provides a simple method for regulating the morphologies of metal oxides to obtain superstructures by the organic metal salt precursors, which have a similar structure of $Zn(DDAB)_2$.

ASSOCIATED CONTENT

Ⓢ Supporting Information

The Supporting Information is available free of charge at https://pubs.acs.org/doi/10.1021/acsomega.1c01841.

> Crystal sizes calculated from XRD patterns; SEM images of a series of ZnO superstructures; TGA curve of twined mushrooms; and Nyquist plots of a series of MeOH−H_2O solvents (PDF)

AUTHOR INFORMATION

Corresponding Authors

Yijiang Shao − *Hefei Technology College, Hefei 238000, China;* ⓞ orcid.org/0000-0003-3897-2932; Email: shaoyijiang@126.com

Yuqiao Wang − *Institute of Advanced Materials, School of Chemistry and Chemical Engineering, Southeast University, Nanjing 211189, China;* ⓞ orcid.org/0000-0001-9281-3911; Email: yqwang@seu.edu.cn

Authors

Bo Song − *Hefei Technology College, Hefei 238000, China; Changzhou Huawei Electronics Co. Ltd., Changzhou 213144, China; Institute of Advanced Materials, School of Chemistry and Chemical Engineering, Southeast University, Nanjing 211189, China;* ⓞ orcid.org/0000-0002-1349-0163

Yun Xie − *Hefei Technology College, Hefei 238000, China*

Xia Cui − *Hefei Technology College, Hefei 238000, China; Changzhou Huawei Electronics Co. Ltd., Changzhou 213144, China; Institute of Advanced Materials, School of Chemistry and Chemical Engineering, Southeast University, Nanjing 211189, China*

Guangyao Zhan − *Changzhou Huawei Electronics Co. Ltd., Changzhou 213144, China*

Jing Mao − *Hefei Technology College, Hefei 238000, China*

Changzeng Fan − *State Key Laboratory of Metastable Materials Science and Technology, Yanshan University, Qinhuangdao 066004, China*

Yueming Sun − *Institute of Advanced Materials, School of Chemistry and Chemical Engineering, Southeast University, Nanjing 211189, China*

Complete contact information is available at:
https://pubs.acs.org/10.1021/acsomega.1c01841

Author Contributions

[⊥]B.S. and Y.X. contributed equally to this work.

Notes

The authors declare no competing financial interest.

ACKNOWLEDGMENTS

REFERENCES

(1) Yang, G. Z.; Song, H. W.; Cui, H.; Liu, Y. C.; Wang, C. X. Ultrafast Li-ion battery anode with superlong life and excellent cycling stability from strongly coupled ZnO nanoparticle/conductive nano-carbon skeleton hybrid materials. *Nano Energy* **2013**, *2*, 579−585.

(2) Sallet, V.; Deparis, C.; Patriarche, G.; Sartel, C.; Amiri, G.; Chauveau, J.-M.; Morhain, C.; Perez, J. Z. Why is it difficult to grow spontaneous ZnO nanowires using molecular beam epitaxy? *Nanotechnology* **2020**, *31*, No. 385601.

(3) Wang, Q.; Zhou, H.; Liu, X.; Li, T.; Jiang, C.; Song, W.; Chen, W. Facet-dependent generation of superoxide radical anions by ZnO nanomaterials under simulated solar light. *Environ. Sci. Nano* **2018**, *5*, 2864−2875.

(4) Miyake, M.; Suginohara, M.; Narahara, N.; Hirato, T.; Braun, P. V. Low-Temperature Hydrothermal Synthesis of Colloidal Crystal Templated Nanostructured Single-Crystalline ZnO. *Chem. Mater.* **2017**, *29*, 9734−9741.

(5) Xu, G.-L.; Li, Y.; Ma, T.; Ren, Y.; Wang, H.-H.; Wang, L.; Wen, J.; Miller, D.; Amine, K.; Chen, Z. PEDOT-PSS coated ZnO/C hierarchical porous nanorods as ultralong-life anode material for lithium ion batteries. *Nano Energy* **2015**, *18*, 253−264.

(6) Peng, W.; Han, L.; Wang, Z. Hierarchically Structured ZnO Nanorods as an Efficient Photoanode for Dye-Sensitized Solar Cells. *Chem. - Eur. J.* **2014**, *20*, 8483−8487.

(7) Shi, Y.; Zhu, C.; Wang, L.; Zhao, C.; Li, W.; Fung, K. K.; Ma, T.; Hagfeldt, A.; Wang, N. Ultrarapid Sonochemical Synthesis of ZnO Hierarchical Structures: From Fundamental Research to High Efficiencies up to 6.42% for Quasi-Solid Dye-Sensitized Solar Cells. *Chem. Mater.* **2013**, *25*, 1000−1012.

(8) Li, F.; Gong, F.; Xiao, Y.; Zhang, A.; Zhao, J.; Fang, S.; Jia, D. ZnO Twin-Spheres Exposed in ±(001) Facets: Stepwise Self-Assembly Growth and Anisotropic Blue Emission. *ACS Nano* **2013**, *7*, 10482−10491.

(9) Liu, Y.; Huang, D.; Liu, H.; Li, T.; Wang, J. ZnO Tetrakaidecahedrons with Coexposed {001}, {101}, and {100} Facets: Shape-Selective Synthesis and Enhancing Photocatalytic Performance. *Cryst. Growth Des.* **2019**, *19*, 2758−2764.

(10) Chetia, T. R.; Ansari, M. S.; Qureshi, M. Rational design of hierarchical ZnO superstructures for efficient charge transfer: mechanistic and photovoltaic studies of hollow, mesoporous, cage-like nanostructures with compacted 1D building blocks. *Phys. Chem. Chem. Phys.* **2016**, *18*, 5344−5357.

(11) Ramu, P.; Anbarasan, P. M.; Ramesh, R.; Aravindan, S.; Ponnusamy, S.; Muthamizhchelvan, C.; Yaakob, Z. Synthesis of dumbbell shaped ZnO crystals using one-pot hydrothermal method and their characterisations. *Mater. Lett.* **2014**, *122*, 230−233.

(12) Cai, X.; Wang, F.; Yan, D.; Zhu, Z.; Gu, X. Luminescence characteristics and growth mechanism of awl-like ZnO Nanostructures fabricated on Ni-coated silicon substrate via chemical vapor deposition method. *Ceram. Int.* **2014**, *40*, 12293−12298.

(13) Akin, B.; Oner, M. Aqueous pathways for formation of zinc oxide particles in the presence of carboxymethyl inulin. *Res. Chem. Intermed.* **2012**, *38*, 1511−1525.

(14) Noriko, S.; Hajime, H. Hierarchical structures of ZnO spherical particles synthesized solvothermally. *Sci. Technol. Adv. Mater.* **2011**, *12*, No. 064707.

(15) Wang, L.; Chang, L.; Zhao, B.; Yuan, Z.; Shao, G.; Zheng, W. Systematic Investigation on Morphologies, Forming Mechanism, Photocatalytic and Photoluminescent Properties of ZnO Nanostructures Constructed in Ionic Liquids. *Inorg. Chem.* **2008**, *47*, 1443−1452.

(16) Jung, M.-H.; Chu, M.-J. Synthesis of hexagonal ZnO nanodrums, nanosheets and nanowires by the ionic effect during the growth of hexagonal ZnO crystals. *J. Mater. Chem. C* **2014**, *2*, 6675−6682.

(17) Zhou, X.; Xie, Z.-X.; Jiang, Z.-Y.; Kuang, Q.; Zhang, S.-H.; Xu, T.; Huang, R.-B.; Zheng, L.-S. Formation of ZnO hexagonal micro-pyramids: a successful control of the exposed polar surfaces with the assistance of an ionic liquid. *Chem. Commun.* **2005**, *44*, 5572−5574.

(18) Wang, Z. L. From nanogenerators to piezotronics—A decade-long study of ZnO nanostructures. *MRS Bull.* **2012**, *37*, 814−827.

(19) Nasajpour, A.; Mandla, S.; Shree, S.; Mostafavi, E.; Sharifi, R.; Khalilpour, A.; Saghazadeh, S.; Hassan, S.; Mitchell, M. J.; Leijten, J.; Hou, X.; Moshaverinia, A.; Annabi, N.; Adelung, R.; Mishra, Y. K.; Shin, S. R.; Tamayol, A.; Khademhosseini, A. Nanostructured Fibrous Membranes with Rose Spike-Like Architecture. *Nano Lett.* **2017**, *17*, 6235−6240.

(20) Matsumoto, K.; Saito, N.; Mitate, T.; Hojo, J.; Inada, M.; Haneda, H. Surface Polarity Determination of ZnO Spherical Particles Synthesized via Solvothermal Route. *Cryst. Growth Des.* **2009**, *9*, 5014−5016.

(21) Peng, F.; Zhou, Q.; Lu, C.; Ni, Y.; Kou, J.; Xu, Z. Construction of (001) facets exposed ZnO nanosheets on magnetically driven cilia film for highly active photocatalysis. *Appl. Surf. Sci.* **2017**, *394*, 115−124.

(22) Tian, S.; Li, N.; Zeng, D.; Li, H.; Tang, G.; Pang, A.; Xie, C.; Zhao, X. Hierarchical ZnO hollow microspheres with exposed (001) facets as promising catalysts for the thermal decomposition of ammonium perchlorate. *CrystEngComm* **2015**, *17*, 8689−8696.

(23) Timpel, M.; Nardi, M. V.; Krause, S.; Ligorio, G.; Christodoulou, C.; Pasquali, L.; Giglia, A.; Frisch, J.; Wegner, B.; Moras, P.; Koch, N. Surface Modification of ZnO(0001)−Zn with

(24) Wang, H.; Xie, C.; Zeng, D.; Yang, Z. Controlled organization of ZnO building blocks into complex nanostructures. *J. Colloid Interface Sci* **2006**, *297*, 570−577.

(25) Chang, J.; Ahmad, M. Z.; Wlodarski, W.; Waclawik, E. R. Self-Assembled 3D ZnO Porous Structures with Exposed Reactive {0001} Facets and Their Enhanced Gas Sensitivity. *Sensors* **2013**, *13*, 8445−8460.

(26) Song, B.; Wang, Y.; Cui, X.; Kou, Z.; Si, L.; Tian, W.; Yi, C.; Wei, T.; Sun, Y. A Series of Unique Architecture Building of Layered Zinc Hydroxides: Self-Assembling Stepwise Growth of Layered Zinc Hydroxide Carbonate and Conversion into Three-Dimensional ZnO. *Cryst. Growth Des.* **2016**, *16*, 887−894.

(27) Wang, L.; Chang, L.-X.; Wei, L.-Q.; Xu, S.-Z.; Zeng, M.-H.; Pan, S.-L. The effect of 1-N-alkyl chain of ionic liquids [Cnmim] + Br⁻ (n = 2, 4, 6, 8) on the aspect ratio of ZnO nanorods: syntheses, morphology, forming mechanism, photoluminescence and recyclable photocatalytic activity. *J. Mater. Chem.* **2011**, *21*, 15732−15740.

(28) Waltz, F.; Wißmann, G.; Lippke, J.; Schneider, A. M.; Schwarz, H.-C.; Feldhoff, A.; Eiden, S.; Behrens, P. Evolution of the Morphologies of Zinc Oxide Mesocrystals Under the Influence of Natural Polysaccharides. *Cryst. Growth Des.* **2012**, *12*, 3066−3075.

(29) Liu, Z.; Wen, X. D.; Wu, X. L.; Gao, Y. J.; Chen, H. T.; Zhu, J.; Chu, P. K. Intrinsic Dipole-Field-Driven Mesoscale Crystallization of Core−Shell ZnO Mesocrystal Microspheres. *J. Am. Chem. Soc.* **2009**, *131*, 9405−9412.

(30) Yu, Q.; Yu, C.; Yang, H.; Fu, W.; Chang, L.; Xu, J.; Wei, R.; Li, H.; Zhu, H.; Li, M.; Zou, G.; Wang, G.; Shao, C.; Liu, Y. Growth of Dumbbell-like ZnO Microcrystals under Mild Conditions and their Photoluminescence Properties. *Inorg. Chem.* **2007**, *46*, 6204−6210.

(31) Cölfen, H.; Antonietti, M. Mesocrystals: Inorganic Super-structures Made by Highly Parallel Crystallization and Controlled Alignment. *Angew. Chem., Int. Ed.* **2005**, *44*, 5576−5591.

(32) Sun, X.; Li, Q.; Jiang, J.; Mao, Y. Morphology-tunable synthesis of ZnO nanoforest and its photoelectrochemical performance. *Nanoscale* **2014**, *6*, 8769−8780.

(33) Limo, M. J.; Ramasamy, R.; Perry, C. C. ZnO Binding Peptides: Smart Versatile Tools for Controlled Modification of ZnO Growth Mechanism and Morphology. *Chem. Mater.* **2015**, *27*, 1950−1960.

(34) Song, B.; Cui, X.; Wang, Y.; Si, L.; Kou, Z.; Tian, W.; Yi, C.; Sun, Y. Controllable Growth of Unique Three-Dimensional Layered Basic Zinc Salt/ZnO Binary Structure. *Cryst. Growth Des.* **2016**, *16*, 4877−4885.

(35) Zhu, H.; Huang, J.-F.; Pan, Z.; Dai, S. Ionothermal Synthesis of Hierarchical ZnO Nanostructures from Ionic-Liquid Precursors. *Chem. Mater.* **2006**, *18*, 4473−4477.

(36) Liu, D.-P.; Li, G.-D.; Su, Y.; Chen, J.-S. Highly Luminescent ZnO Nanocrystals Stabilized by Ionic-Liquid Components. *Angew. Chem.* **2006**, *118*, 7530−7533.

(37) Nikoobakht, B.; El-Sayed, M. A. Evidence for Bilayer Assembly of Cationic Surfactants on the Surface of Gold Nanorods. *Langmuir* **2001**, *17*, 6368−6374.

(38) Fan, L.; Guo, R. Growth of Dendritic Silver Crystals in CTAB/SDBS Mixed-Surfactant Solutions. *Cryst. Growth Des.* **2008**, *8*, 2150−2156.

(39) Zeng, H.; Cai, W.; Liu, P.; Xu, X.; Zhou, H.; Klingshirn, C.; Kalt, H. ZnO-Based Hollow Nanoparticles by Selective Etching: Elimination and Reconstruction of Metal−Semiconductor Interface, Improvement of Blue Emission and Photocatalysis. *ACS Nano* **2008**, *2*, 1661−1670.

(40) Zeng, H.; Li, Z.; Cai, W.; Liu, P. Strong localization effect in temperature dependence of violet-blue emission from ZnO nano-shells. *J. Appl. Phys.* **2007**, *102*, No. 104307.

(41) Dai, J.; Yuan, M.-H.; Zeng, J.-H.; Dai, Q.-F.; Lan, S.; Xiao, C.; Tie, S.-L. Three-photon-induced blue emission with narrow bandwidth from hot flower-like ZnO nanorods. *Opt. Express* **2015**, *23*, 29231−29244.

(42) Baranwal, V.; Zahra, A.; Singh, P. K.; Pandey, A. C. Starch assisted growth of dumbbell-shaped ZnO microstructures. *J. Alloys Compd.* **2015**, *646*, 238−242.

(43) Gerigk, M.; Ehrenreich, P.; Wagner, M. R.; Wimmer, I.; Reparaz, J. S.; Sotomayor Torres, C. M.; Schmidt-Mende, L.; Polarz, S. Nanoparticle shape anisotropy and photoluminescence properties: Europium containing ZnO as a Model Case. *Nanoscale* **2015**, *7*, 16969−16982.

(44) Zeng, H.; Duan, G.; Li, Y.; Yang, S.; Xu, X.; Cai, W. Blue Luminescence of ZnO Nanoparticles Based on Non-Equilibrium Processes: Defect Origins and Emission Controls. *Adv. Funct. Mater.* **2010**, *20*, 561−572.

(45) Cai, M. Z.; Mao, W.; Calvez, L.; Rocherulle, J.; Ma, H. L.; Lebullenger, R.; Zhang, X. H.; Xu, S. Q.; Zhang, J. J. Broadband blue emission from ZnO amorphous nanodomains in zinc phosphate oxynitride glass. *Opt. Lett.* **2018**, *43*, 5845−5848.

(46) Ghamsari, M. S.; Alamdari, S.; Razzaghi, D.; Arshadi Pirlar, M. ZnO nanocrystals with narrow-band blue emission. *J. Lumin.* **2019**, *205*, 508−518.

(47) Yamamoto, A.; Moriwaki, Y.; Hattori, K.; Yanagi, H. A comparative study of photoluminescence of Zn-polar and O-polar faces in single crystal ZnO using moment analysis. *Appl. Phys. Lett.* **2011**, *98*, No. 061907.